VOL. 8, NO. 9, SEPTEMBER 2013 ISSN 1819-6608
ARPN Journal of Engineering and Applied Sciences

www.arpnjournals.com

# A NEW METHODOLOGY TO ESTIMATE DEFORMATION OF LONGITUDINAL SAFETY BARRIERS

Marco Guerrieri[1], Giuseppe Parla[2], Ferdinando Corriere[2]
[1] Faculty of engineering and Architecture, University of "Enna" Kore, Italy
[2]Faculty of engineering, University of Palermo, Italy
E-mail: marco.guerrieri@tin.it

**ABSTRACT**

This paper presents a new high-efficiency methodology to estimate deformations of longitudinal road safety barriers, whose monitoring is a necessary condition for the maintenance of high safety standards. The methodology is based on the analysis of videotaped sequences, obtained by means of two matched video cameras ("stereo head") installed on a vehicle adequately equipped. Two different theoretical approaches have been defined: monoscopic and stereoscopic. The new methodology has been used to empirically evaluate the longitudinal safety barrier deformations on an Italian road.

**Keywords:** Longitudinal barrier, deformations, stereoscopic, image processing

## DETECTION OF ROAD BARRIERS

The first stage of procedure to estimate deformation of longitudinal safety barriers has been devoted to detect the extrados line in safety barriers; the Canny algorithm [1, 2] has then been used to reduce the image noise (edge detection). The Canny algorithm studies in detail the behavior of the gradient operator applied to a noisy edge. As a matter of fact this algorithm presupposes that the image edge front to be segmented is already corrupted by Gaussian white noise; therefore, such an algorithm convolves the image to be processed with a suitable Gaussian smoothing filter so as to meet the following conditions [1, 3, 4, 5, 6]:

- high probability of detecting the real edge;
- the image points highlighted by the gradient operator must be as faithful as possible to the real edge of the object under examination;
- uniqueness of the answer (exclusion of any multiple edges of the object).

The algorithm can be divided into different steps:

- image Gaussian smoothing, applied separately to the two directions (x, y), to reduce the noise;
- pixel gradient calculation;
- thresholding or non-maximum suppression in longitudinal direction to the edge which utilizes two different threshold values. Such a phase is useful to distinguish the most marked (significant) edge points from those less marked (weak);
- thinning (significant edge selection through hysteresis) which allows to eliminate or not some weak edge points in relation to the direction and the intensity of the gradient of the points adjacent to the angle.

The high quality of the results from the Canny method can be justified by the fact that the method utilizes two thresholds, one for detecting the sharpest edges, the other for detecting the weakest edges.

The latter are, however, taken into consideration only if they appear to be connected to "sharp" edges. Therefore, in Canny algorithm, the traditional single-threshold-based needs to be replaced with a double-threshold-based approach called hysteresis thresholding; the latter is employed after applying the non-maximum suppression.

In particular, if we determine the two thresholds $t_1$ and $t_2$ as $t_1>t_2$, the algorithm establishes that the pixel located at position (i,j) on the generic chromatic plane p of the image A(i,j,p) is a Canny edge pixel if the intensity value of the pixel examined - A(i,j,p) – appears to be superior to the highest threshold value t1; while the lowest value $t_2$ indicates the limit under which the pixel is not a Canny edge without any doubt.

Moreover, the algorithm determines that the pixel set with values ranging between $t_1$ and $t_2$ are edged only if they are connected to those certainly edged, or those whose value is higher than $t_1$. The above can be summed up into the following inequalities:

$$\begin{cases} \mathbf{A(i,j,p) > t1} \\ \text{then A(i,j,p) are edged} \\ \mathbf{t2 \geq A(i,j,p) \geq t1} \\ \text{then A(i,j,p) are defined as rough edges} \\ \mathbf{A(i,j,p) > t2} \\ \text{then A(i,j,p) isn't an edge} \end{cases} \quad (1)$$

It has also been observed that on the same image, an edge detection applied separately to the three chromatic planes (RGB) [1] produces, as expected, nearly similar results. In addition, the edges in all the objects in the scene, provided from the previous segmentation, differ in a few pixels only if the segmented images on the three planes are separately elaborated or the threshold results are grouped in a single plane, or else if the elaboration is done on a grey-scale image obtained by appropriately converting a color image. For these reasons we preferred to operate separately on the three chromatic image planes and group the processing results into one Boolean piece of information.

The procedure described has been applied to an Italian road into operation with safety barriers deformed from accidents. Fig. 1 shows the barrier as already corrected and will be later discussed, while Fig. 2 illustrates the binary image obtained through Canny algorithm.

**Figure - 1.** Initial image

**Figure - 2.** Binary image obtained from Canny algorithm.

For each point {C} of the determined edges, suitable convolution masks and congruence imposed on the chromatic intensities will help to:

- determine the gradient direction;
- create, for the eight pixels adjacent to each edge point, two brighter {A} and less bright {B} sets; an example of the pixel matching procedure to such sets is given by pixel intensities in the image shown in Figure 3;
- eliminate any pixel belonging to {A} and {B} at the same time;
- impose congruence of the result on the previous step with Canny edge {C}.

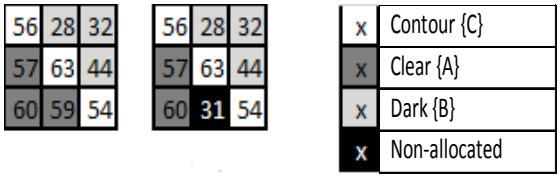


**Figure - 3.** Matching to sets {A} and {B}

**Figure - 4.** Binary image without discontinuity

This way the edges become slightly thickened, thus closing (by connectivity) and eliminating any discontinuity in the extrados points of the safety barrier (see Fig. 4). The set of points obtained populate the dominion {C} which appears to be modified in comparison with the initial Canny
information [3]. The next stage has been devoted to the individuation and isolation of the extrados line of the barrier starting from the information contained in the binary image [6, 7, 8] in Figure 4. This image encodes all the present objects in a binary format and is acquired by the algorithm to extract the rectilinear segments which detect the edge lines of every object of interest. In order to eliminate any defect caused by occlusion or noise, the polylines [2] processed by the algorithm in this stage are then subject to be controlled by such criteria as the distance between parallel rectilinear segments and their orientation towards the reference horizontal plane parallel to the x axis (image axis). A set of functions of geometric congruence is crucial to selecting the groups of polylines which should be analyzed stereoscopically or may represent the ridge line of the safety barrier, then formalized through relation (2).

$$CG(i,j) = F_{geometria}(C(i,j)) \quad (2)$$

The algorithm, therefore, extracts each binary object contained in domain {C} and by means of relation (2) identifies the ridge line of the barrier as shown in Figure 5.

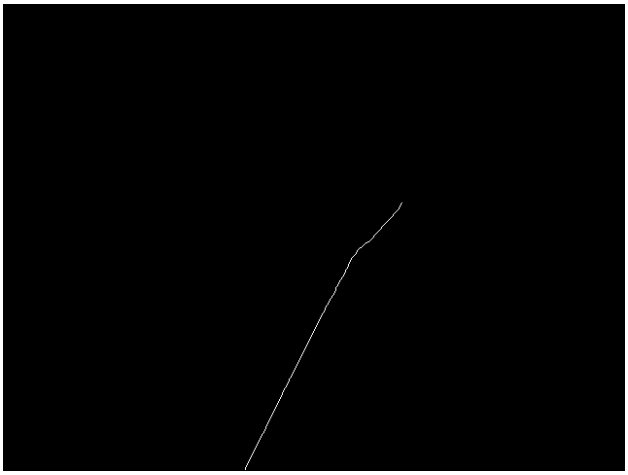

**Figure - 5.** Top edge contour of the barrier

## STEREOSCOPIC APPLICATION

Stereoscopy is based on the analysis of images coming from two video cameras located at a certain distance between each other, called baseline [4, 5, 9, 11, 12, 13].

The object pixels shown in the image pairs appear with small relative shifts and therefore the images acquired by the stereo vision system have slightly different viewpoints. By exploiting this condition, by means of a stereo triangulation [10, 11, 12 e 13], it is possible to calculate the depth and therefore the real dimensions of the objects portrayed. In order to simplify the processing, it is undoubtedly crucial that the two video cameras are endowed with lenses of the same focal length and that the sensors have equally sized pixels.

In general, the images recorded by video cameras can contain some noise levels which may nullify the search for correspondences between the same objects in both images.

To this end some corrections are made to eliminate such distortions in each left or right image, recorded by the stereo system. The correction procedures belong to a preliminary calibration process of the video cameras which is synthetically described below.

In an ideal environment stereo head cameras answer the pinhole model and therefore have exactly the same focal length and perfectly parallel optical axes. As a matter of fact, the lenses unfortunately introduce some distortions and may have different focal lengths and misaligned optical axes.

The calibration objective [10, 14] is to determine two sets of parameters, intrinsic and extrinsic, which compensate for the imperfection in the stereo head.

The intrinsic parameters correct lens distortions and focal length difference, while the extrinsic ones determine the spatial offset of both video cameras, including the distance between them and the deviation from the parallelism of the optical axes.

Such parameters allow the images acquired to be transformed into "ideal" images, as those seen from pinhole video cameras with optical axes perfectly parallel. Indeed, in order to facilitate the search for correspondences between the points of the barrier extrados in the left and right images, the images have been corrected by the stereo head extrinsic and intrinsic parameters already known, as illustrated in the following Figures 6 and 7.

The most general form of the perspective projection matrix can be written in the following relation (3) [10]:

$$\tilde{P}_{new} = A \cdot [\mathrm{I}|0] \cdot G = A \cdot [R|T] \tag{3}$$

Where:

$$A = \begin{bmatrix} f \cdot k_u & 0 & u_0 \\ 0 & f \cdot k_v & v_0 \\ 0 & 0 & 1 \end{bmatrix} \tag{4}$$

While R and T are respectively the translation vector and the rotation vector derived from the preliminary calibration procedure.

$$\mathrm{R} = \begin{bmatrix} r_1{}^T \\ r_2{}^T \\ r_3{}^T \end{bmatrix} \tag{5}$$

$$\mathrm{T} = \begin{bmatrix} t_1 \\ t_2 \\ t_3 \end{bmatrix} \tag{6}$$

Matrix A (4) encodes the intrinsic parameters ($f$, $k_u$, $k_v$,$u_0$, $v_0$) of the video camera, on the other hand matrix G encodes the extrinsic parameters (R (5) and T(6)). The $\tilde{P}_{new}$ represents the Perspective Projection Matrix (PPM) which regulates the projection of space points (referred to the system-world) onto the image plane. In the case under examination, downstream of the rectification procedure (Figures 6 and 7), the two perspective transformed images have been determined and the image pairs generating the 3D have been rectified.

**Figure - 6.** Left image rectified

**Figure - 7.** Right image rectified

Once the images have been rectified, the following stage is to compute the correspondences only for extrados points (see relation (2)) of the safety barrier captured in the left and the right images, respectively.

Even if this procedure is described in the previous paragraph, it represents the first stage, downstream of image rectification, which allows to limit the computational load related to the complex determination of the pixel correspondences in the same object in the left and right images.

Indeed, more in general, the first problem to be faced in the 3D construction is the correspondence, that is the search for the projection of the same physical point onto both images (matching point search). This problem is handled with global or local methods.

Through local methods one image is analyzed to find the correspondence with a small region coming from the other. This analysis is carried out on the basis of such features as angles or rectilinear segments (in feature-based methods) or by means of correlation operators (in area-based methods). Global methods integrate local methods with general pieces of information like surface continuity or the presence of peculiar textures in the scene.

Each method for correspondence search has its own characteristics which make it more suitable for some contexts. Feature-based methods, for instance, are particularly effective inside buildings, where the environment contains a great deal of rectilinear surfaces, while area-based techniques allow to deal with a larger range of contexts. The correct and rapid correspondence estimation is mathematically and computationally complex. The main difficulties which may lead to an erroneous association of two non-corresponding points, are due to:

- **occlusions:** the video cameras are located in different positions, therefore some objects may be visible only in either image, or only in a part of it;
- **distortions:** because of the perspective projection, the same object can be differently projected onto both images;
- **different camera parameters:** if one video camera is not focused at the same distance as the other or if their diaphragm opening is different, the corresponding points show distinctive features in every image;
- **specular reflections;**
- **sensor noise.**

In this paper, by taking the surface continuity of the barrier and the uniform colorimetric barrier surface into consideration, an algorithm has been implemented in the point correspondence search, by mutual correlation, between the left and right image (area based), with a constant-size window with 11 rows and 11 columns.

Actually, in order to simplify the global computational load, the windows have been centered along all the edge points determined by relation (2) in the stereo image pairs under analysis. In the next stage the stereoscopic triangulation has been carried out as synthetically explained in the following paragraph.

## STEREOSCOPIC TRIANGULATION

The possibility of detecting an object distance is extremely important in this paper. Indeed, only a tridimensional analysis of the safety barrier dominion in its real form and dimension may lead to inferences about its functional efficiency state.

The simplest case of 3-D search occurs in presence of a canonical stereo system, that is when the corresponding images have no distortions and are perfectly coplanar and aligned by pixel line, with perfectly parallel axes, coinciding focal lengths and so calibrated main points cL and cR that are at the same pixel coordinates in both images. Such an array, called fronto-parallel, is shown in Fig.8 [10, 11,12 e 13].

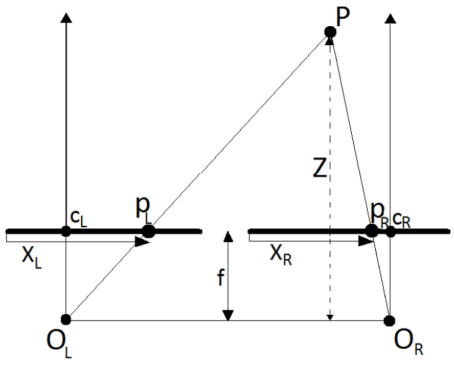


**Figure - 8.** Stereo system

As aforesaid, the straight line connecting the optical centers $O_L$ and $O_R$ of the two video cameras is called *baseline*. For each point P in the space, detected by both the cameras, the disparity is given by the difference between the abscissas $X_L$ and $X_R$ in the coordinate systems on the image plane which originate at the top left-hand side of the two images. By means of a simple geometrical analysis of Figure 8, depth Z is deduced as inversely proportional to the disparity $X_L - X_R$.

When distance Z is short, there is a very big disparity and therefore a high resolution compared to the depth; it is the opposite in case of long distances. More in general (Figure 9) [10], the stereo-triangulation is the

methodology which allows to estimate the 3D point position in the space world starting from the pixel coordinates of its projections onto the retinal sensor planes.

Given the perspective projection matrices, which regulate the projection of a coordinate point w (*see* Figure 9) onto the two image planes, and given the homogeneous pixel coordinates of its projections, the w position can be obtained by intersecting optical rays associated to the planes.

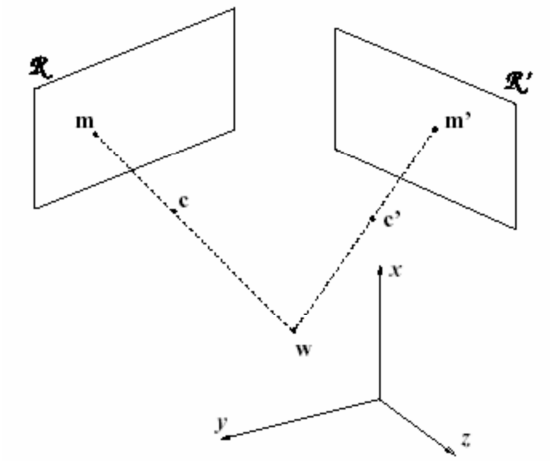


**Figure - 9.** Axonometric projection of the conjugate points in the stereoscopic triangulation process

By systematizing (relation 7) the parametric equations of the straight lines which describe the optical rays, it is possible to determine the position of a generic point in the space-world.

$$\begin{cases} w = c_1 + \lambda_1 + (A_n \cdot R_n)^{-1} \cdot \widetilde{m}_{n1} \\ w = c_2 + \lambda_2 + (A_n \cdot R_n)^{-1} \cdot \widetilde{m}_{n2} \end{cases} \quad (7)$$

Where [10] are the matrices of projection, rotation and the positions of optical centers in which the two perspective projection matrices can be subdivided and obtained downstream of the rectification.

Matrices *An* and *Rn* are the new matrices resulting from the rectification and the coordinates and are the new *w* projections onto the retinal planes after the rectifying transformations and the compensation for radial and tangential distortions.

Relation (7) constitutes an overdetermined system of six equations in five unknown values (three for *w* coordinates plus two free parameters, whose least-squares solution can be achieved through the pseudo inverse method [10].

However, since the least-squares solution has no geometrical meaning, in order to solve relation (7) it is advisable to detect the *w* position as that point with the minimum Euclidean distance between the skew lines describing the optical rays. In fact, it is extremely unusual that the two optical rays intersect exactly at the same point. In light of the latter consideration it is possible to determine the coordinates of a generic point in the world, denoted as follows:

$$w_{sinistra} \begin{bmatrix} x_1 \\ y_1 \\ z_1 \end{bmatrix} \quad (8)$$

$$w_{sdestra} \begin{bmatrix} x_2 \\ y_2 \\ z_2 \end{bmatrix} \quad (9)$$

$$\widehat{w} = \frac{w_{sinistra} + w_{destra}}{2} \quad (10)$$

The above described procedure has obviously been applied only to some image pairs where the relative configuration between the positions of the video cameras and the barriers (straightly and horizontally) allows the 3D determination for all the points of the profile looked for.

Given the points $\widehat{w}$ (see eq. 10) of the extrados of the barrier portrayed, they have been compared with the theoretical undeformed profile just next to the damaged area as illustrated in the following Figure 11:

**Figure - 10.** Comparison between the two profiles just at the barrier distortion

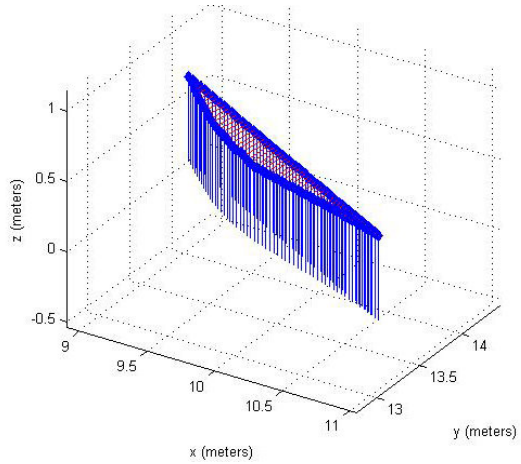


**Figure - 11.** 3D comparison between the two profiles just at the barrier deformation

Moreover the shift analysis between the two 3D profiles has allowed to examine separately the two shift components in the two main planes XY and XZ according to what is illustrated in the following figure.

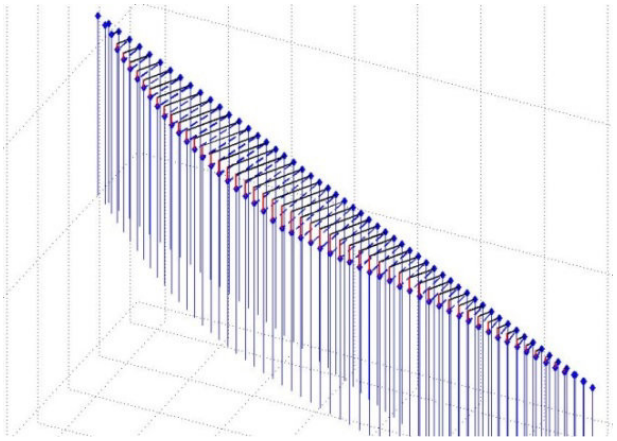

**Figure - 12.** Decomposition of minimum distance vectors into the two compared profiles

Through 3D analysis (*see* Fig. 12) by means of projection onto the planes XY and XZ transversal and vertical distortions of the deformed barrier, in comparison with the original configuration, have been obtained. A similar method of analysis can also be used for safety barriers installed at traditional and innovative road intersections [15, 16, 17, 18, 19, 20].

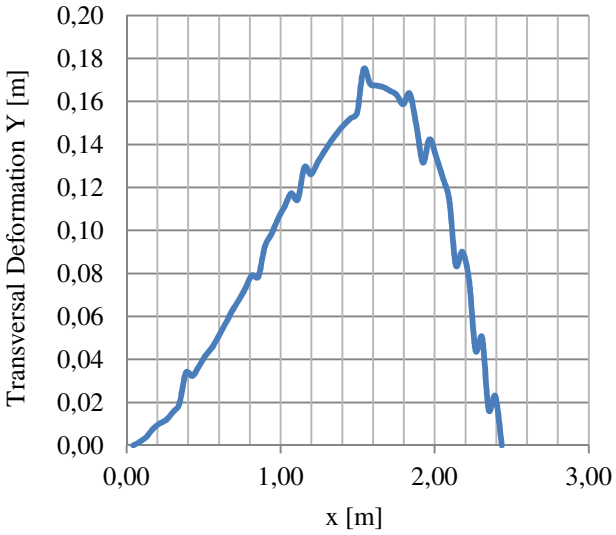


**Figure - 13.** Deformation on the plane XY

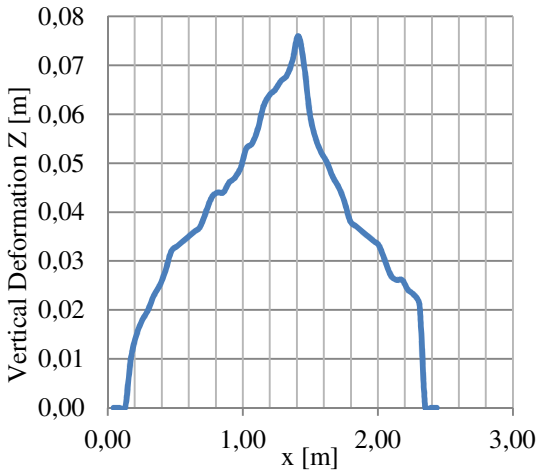


**Figure - 14.** Deformation on the plane XZ

## CONCLUSION

The paper presents an innovative high-efficiency methodology to estimate the deformations of road safety barriers. The image processing procedure adopted is based on videotaped sequences obtained by employing two matched video cameras ("stereo head") installed in an automated vehicle. The mathematical algorithms obtained from theoretical treatment, especially those concerning 3D analysis of the barriers, allow to evaluate the transversal and vertical deformations in a very precise and quick manner. The method is thus suitable for the implementation in the public and/or private administrations which manage road infrastructures in order to monitor barriers and consequently to guarantee adequate passive road safety levels.

## REFERENCES

[1] Canny, J. (1986) A Computational Approach to Edge Detection. IEEE T Pattern Anal, 8(6):679–698.

[2] Rousseeuw, P. J. and Leroy, A. M. (1987). Robust Regression and Outlier Detection, John Wiley & Sons, New York.

[3] Bruno L, Parla G, Celauro C (2011). Image analysis for detecting aggregate gradation in asphalt mixture from planar images. CONSTRUCTION AND BUILDING MATERIALS, vol. 1, p. 21-30, ISSN: 0950-0618, doi: 10.1016/j.conbuildmat.2011.08.007

[4] Guerrieri M., Parla G. and Ticali D. (2012). Mono and stereoscopic image analysis for detecting the transverse profile of worn-out rails. Procedia - Social and Behavioral Sciences, Volume 53, 3 October 2012, Pages 611-621, ISSN: 1877-0428

[5] Guerrieri M., Parla G. and Ticali D. (2012). A theoretical and experimental approach to reconstructing the transverse profile of worn-out

rails. Ingegneria Ferroviaria , January 2012, (pp. 23-37), ISSN: 0020-0956.

[6] Freeman, H. (1961). On the encoding of arbitrary geometric configurations. Ire trans. Electron.comput. EC-10.

[7] Xavier, T. et. Al. Geometric parameters computation with freeman code. Submitted to image anal stereol, 6 pages.

[8] Gonzales, R. C., et. Al. (2004), "Digital image processing using matlab" – Prentice Hall, Upper Saddle River., 2004

[9] Guerrieri, M., Parla, G., Ticali, D., Corriere, F. (2012). Tramway Track: a New Approach for Measuring the Transverse Profile of Worn-Out Rails" AASRI Procedia Journal - Volume 3, Pages 451-456, ISSN: 2212-6716. Elsevier.

[10] A. Fusiello, "Visione artificiale: appunti delle lezioni", Dipartimento di Informatica, Università di Verona, 2003

[11] Hartley R., Zisserman A. (2003). Multiple View Geometry in Computer Vision 2nd edition. Cambridge University Press, 2003.

[12] Hartley R., Zisserman A. (2000). Multiple View geometry in Computer Vision. Cambridge University Press, 2000.

[13] Faugeras O. (1993). Three-Dimentional Computer Vision. MIT Press, Cambridge, MA (pp. 33-68).

[14] Zhang Z. (1998). Determining the epipolar geometry and its uncertainty: A review. International Journal of Computer Vision, 27(2), (pp. 161-195).

[15] Corriere, F., Di Vincenzo, D., Guerrieri, M. (2013). A stochastic decision process model for optimization of railway and tramway track maintenance by means of image processing technique", European Journal of Scientific Research, ISSN: 1450-216X/1450-202X , April 2013, Vol. 99, n.1, pp. 47-56

[16] Corriere, F., Guerrieri, M., Ticali, D., Messineo, A. (2013). Estimation of air pollutant emissions in Flower roundabouts and in conventional roundabouts. Archives of Civil Engineering. Volume 59, Issue 2, Pages 229–246, ISSN (Print) 1230-2945, DOI: 10.2478/ace-2013-0012, July 2013

[17] Mauro, R., Guerrieri, M. (2013). Flower roundabouts: performances analysis and comparison with conventional layouts. European Journal of Scientific Research, ISSN: 1450-216X/1450-202X , Volume 94 Issue 2, January, pp. 242-252, EuroJournals Publishing, Inc. 2012.

[18] Mauro, R., Guerrieri, M. (2013). Right-turn bypass lanes at roundabouts: geometric schemes and functional analysis. Modern Applied Science, ISSN 1913-1844 (Print) ISSN 1913-1852 (Online), Canadian Center of Science and Education, Vol. 7, No. 1, January 2013 (pp. 1-12). DOI: 10.5539/mas.v7n1p1

[19] Guerrieri, M., Corriere, F., Ticali, D. (2012). Turbo-roundabouts: a model to evaluate capacity, delays, queues and Level of Service. European Journal of Scientific Research, ISSN: 1450-216X/1450-202X , Volume 92 Issue 2, December 2012, pp. 267-282, EuroJournals Publishing, Inc. 2012.

[20] Corriere, F., Guerrieri, M. (2012). Performance analysis of basic turbo-roundabout in urban context. Procedia - Social and Behavioral Sciences, Volume 53, 3 October 2012, Pages 622-632, ISSN: 1877-0428